

RESEARCH ARTICLE

10.1002/2014GC005563

Development and evolution of detachment faulting along 50 km of the Mid-Atlantic Ridge near 16.5°N

Special Section:

Oceanic Detachment Faults

Key Points:

- Study provides new insights into oceanic detachment faults
- Several morphologic expressions of oceanic detachment faulting are described
- Relationship between detachment faulting and axial volcanism is examined

Correspondence to:

D. K. Smith,
dsmith@whoi.edu

Citation:

Smith, D. K., et al. (2014), Development and evolution of detachment faulting along 50 km of the Mid-Atlantic Ridge near 16.5°N, *Geochem. Geophys. Geosyst.*, 15, 4692–4711, doi:10.1002/2014GC005563.

Received 28 AUG 2014

Accepted 12 NOV 2014

Accepted article online 18 NOV 2014

Published online 5 DEC 2014

Deborah K. Smith¹, Hans Schouten¹, Henry J. B. Dick¹, Johnson R. Cann², Vincent Salters³, Horst R. Marschall¹, Fuwu Ji⁴, Dana Yoerger¹, Alessio Sanfilippo⁵, Ross Parnell-Turner⁶, Camilla Palmiotto⁷, Alexei Zheleznov⁸, Hailong Bai⁹, Will Junkin⁹, Ben Urann¹, Spencer Dick¹⁰, Margaret Sulanowska¹, Peter Lemmond¹, and Scott Curry¹

¹Department of Geology and Geophysics, Woods Hole Oceanographic Institution, Woods Hole, Massachusetts, USA, ²School of Earth and Environment, University of Leeds and Curlew Cottage, Penrith, UK, ³Department of Geological Sciences, Florida State University, Tallahassee, Florida, USA, ⁴School of Ocean and Earth Science, Tongji University, Shanghai, People's Republic of China, ⁵Department of Earth and Environmental Sciences, University of Pavia, Pavia, Italy, ⁶Bullard Laboratories, Department of Earth Sciences, University of Cambridge, Cambridge, UK, ⁷Istituto di Scienze Marine, ISMAR-CNR, Bologna, Italy, ⁸Department of Geomorphology, Institute of Earth Sciences, Saint Petersburg State University, St. Petersburg, Russia, ⁹Department of Geology, University of Maryland, College Park, Maryland, USA, ¹⁰Geology and Geography Department, Ohio Wesleyan University, Delaware, Ohio, USA

Abstract A multifaceted study of the slow spreading Mid-Atlantic Ridge (MAR) at 16.5°N provides new insights into detachment faulting and its evolution through time. The survey included regional multibeam bathymetry mapping, high-resolution mapping using AUV *Sentry*, seafloor imaging using the *TowCam* system, and an extensive rock-dredging program. At different times, detachment faulting was active along ~50 km of the western flank of the study area, and may have dominated spreading on that flank for the last 5 Ma. Detachment morphologies vary and include a classic corrugated massif, noncorrugated massifs, and back-tilted ridges marking detachment breakaways. High-resolution *Sentry* data reveal a new detachment morphology; a low-angle, irregular surface in the regional bathymetry is shown to be a finely corrugated detachment surface (corrugation wavelength of only tens of meters and relief of just a few meters). Multiscale corrugations are observed 2–3 km from the detachment breakaway suggesting that they formed in the brittle layer, perhaps by anastomosing faults. The thin wedge of hanging wall lavas that covers a low-angle (6°) detachment footwall near its termination are intensely faulted and fissured; this deformation may be enhanced by the low angle of the emerging footwall. Active detachment faulting currently is limited to the western side of the rift valley. Nonetheless, detachment fault morphologies also are present over a large portion of the eastern flank on crust >2 Ma, indicating that within the last 5 Ma parts of the ridge axis have experienced periods of two-sided detachment faulting.

1. Introduction

Normal faults at slower spreading ridges may have very large offsets (tens of km to greater than a hundred km) and account locally for 60–100% of the plate separation [e.g., Baines *et al.*, 2008; Cannat *et al.*, 2006; Grimes *et al.*, 2008; Ohara *et al.*, 2001; Okino *et al.*, 2004; Searle *et al.*, 2003; Smith *et al.*, 2006, 2008; Tucholke *et al.*, 1998]. These long-lived, large-offset faults (commonly referred to as detachment faults) exhume lower crustal and upper mantle rocks. As multibeam bathymetry data coverage increases, significant advances in our understanding of detachment faults are being made. A number of different morphologies are now associated with oceanic detachment faulting. These include the well-known domed, corrugated detachment surfaces, noncorrugated massifs, highly back-tilted fault breakaways, and broad smooth hills [Cann *et al.*, 1997; Cannat *et al.*, 2006; Dick *et al.*, 2003; MacLeod *et al.*, 2009; Schroeder *et al.*, 2007; Smith *et al.*, 2008; Tucholke *et al.*, 1998]. In addition, detachment fault formation is not restricted to the ends of spreading segments; detachment faults form anywhere along the length of a segment [e.g., Cannat *et al.*, 2006; Smith *et al.*, 2006, 2008], and may link along axis over a significant portion of a ridge segment [e.g., Reston and Ranero, 2011; Smith *et al.*, 2008].

Spreading by detachment faulting may dominate a region for several millions of years and generate broad expanses of seafloor [Cannat *et al.*, 1995; Escartin *et al.*, 2008; Schroeder *et al.*, 2007]. Escartin *et al.* [2008]

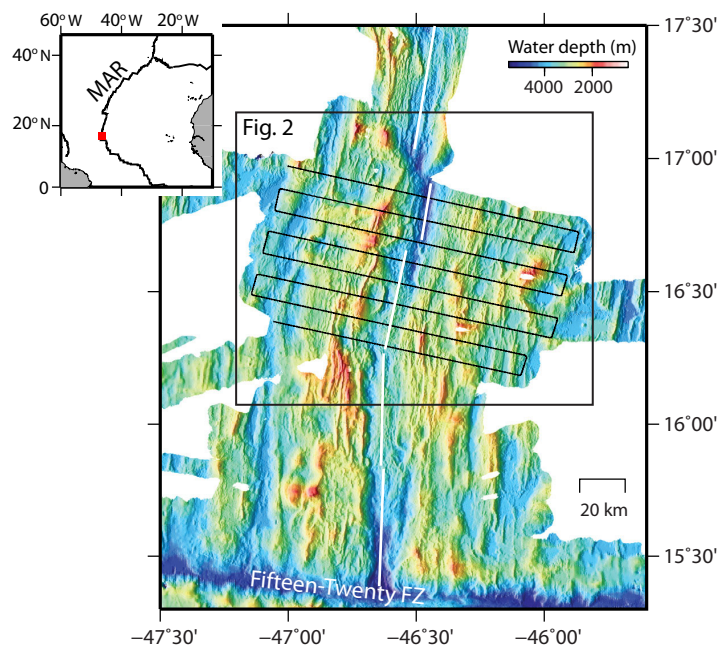


Figure 1. Bathymetric map of the MAR in the 16.5°N region. Inset shows the location of the study area. Black lines: track lines of the regional survey. Black rectangle: area shown in Figure 2.

estimated that active detachment faulting occurs along close to 50% of the northern MAR axis between 12.5°N and 35°N implying that as much as 25% of new seafloor in this region may be formed by detachment faulting. *Smith et al.* [2008] estimated that detachment fault morphologies cover >60% of the seafloor on the west flank of the 13°N segment of the MAR. More recently, it has been suggested that the occurrence of detachment faults may be even more widespread if their surfaces are masked by rafted blocks [*Reston and Ranero, 2011*].

The formation of detachment faults is likely dependent on a balance between several factors, but magma input has

always been considered a key variable. Modeling suggests that detachment faults may form primarily when the fraction of plate separation (M) taken up by magma accretion is between ~ 0.3 and 0.5 [*Buck et al., 2005; Olive et al., 2010; Tucholke et al., 2008*]. If this is the case, then in regions of the MAR where corrugated detachment faults form in the presence of large axial volcanic ridges (AVRs) [e.g., *Smith et al., 2008*], M is likely to be at the high end of the range (0.5), so that 50% of the extension would be taken up by detachment faulting and 50% by magmatic accretion and minor small-offset faulting.

In this paper, we investigate the formation and evolution of detachment faulting in the 16.5°N area of the slow spreading MAR (Figure 1), where detachment faulting has dominated the western flank of the axis for several millions of years. Regional multibeam bathymetry, gravity, and magnetic data were collected out to about 60 km (~ 5 Ma) on each side of the ridge axis. In addition, AUV *Sentry* collected high-resolution multibeam bathymetry, side scan, magnetic, CHIRP, and water column data during 14 dives. Seafloor photographs were obtained using the *TowCam* imaging system during nine tows, and an extensive dredging program was conducted. The 16.5°N study area presents excellent examples of several different morphologic expressions of detachment faulting. Here we assess the different seafloor styles associated with detachment faults, where detachment faults are active, how they evolve off axis, and their relationship to volcanism at the ridge axis.

2. Background

The 16.5°N study area is located ~ 100 km north of the Fifteen-Twenty fracture zone (Figure 1). Previous work identified two distinctive narrow ridges (East and West Ridges, Figure 2) on the western side of the axis as the rotated breakaways of normal faults [*Smith et al., 2008*]. East Ridge, which is closer to the volcanic axis, was interpreted as a newly emerging normal fault forming a rafted block on top of the older West Ridge detachment fault. Seafloor photographs from a camera tow near the top of East Ridge show steep fault scarps cutting pillow lavas on the upper section of the 30° inward-facing slope [*Smith et al., 2008*]. On the 20° outward-facing slope, however, more or less equant pillows are observed. Because pillows that erupt onto steep slopes are typically elongate, *Smith et al.* [2008] suggested that these equant pillows were erupted on the subhorizontal surface of the rift valley floor, faulted, and rotated outward. These observations support the idea that East Ridge marks the breakaway of a rotated fault. *Smith et al.* [2008] also suggested that if mass wasting has not significantly modified the geometry of East Ridge, then the inward-

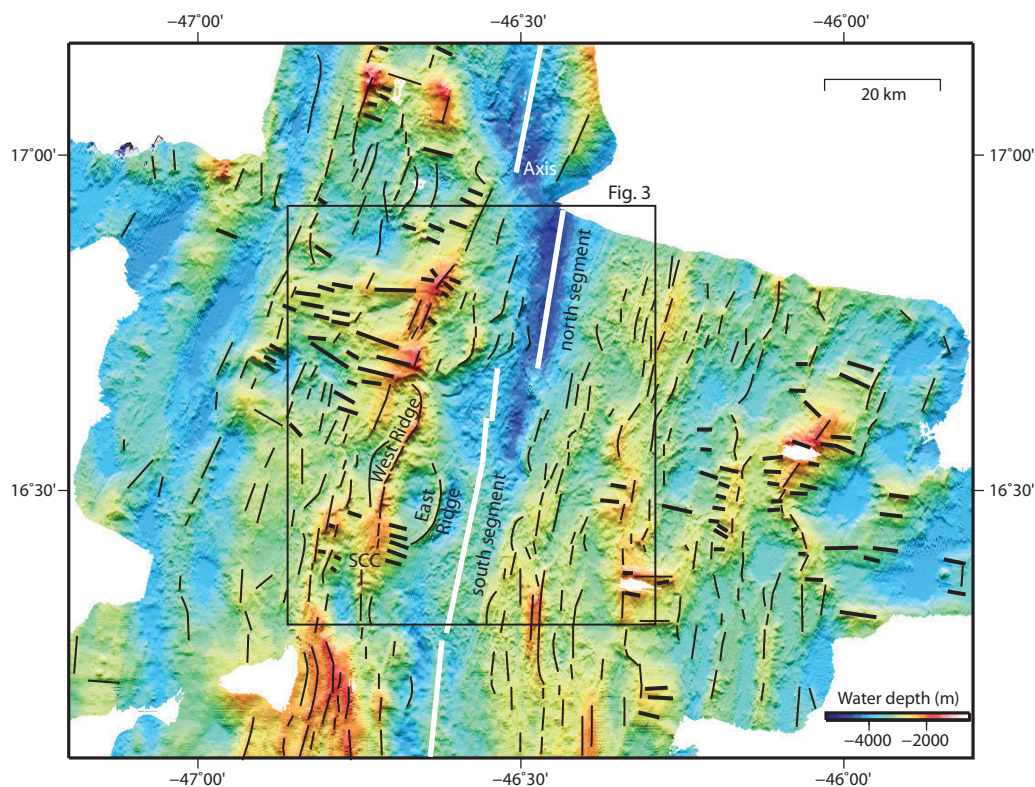


Figure 2. Topographic lineation map. Topographic lineations indicated by thin black lines were identified by eye in the multibeam bathymetry data. Thick black lines mark lineations that we infer are corrugations formed during slip on long-lived faults. White lines: ridge axis. SCC: South Core Complex. Black rectangle: area shown in Figure 3.

facing slope represents a normal fault with an initial dip angle of between 50° and 60° (obtained by summing the inward and outward dips). West Ridge has an outward-facing slope of 35° – 40° , and unpublished photographs obtained over West Ridge show pillow basalts on its top and steep scarps on its inward-facing slope (cruise AT4-4, D.K. Smith chief scientist) supporting its identification as a highly back-tilted fault. The corrugated massif at the south end of West Ridge was identified as a core complex.

The 16.5°N region has a high rate of seismic activity. There are 44 teleseismic earthquakes listed in the NEIC catalog (<http://earthquake.usgs.gov/earthquakes/eqarchives/epic/>) between $16^\circ12'\text{N}$ and 17°N that have magnitudes ≥ 4.5 . In addition, 391 hydroacoustically recorded earthquakes were identified during 4 years of monitoring [Smith *et al.*, 2003], yielding a remarkable average of about one earthquake (roughly $>$ magnitude 2.5–3.0), every 3 days. Based on seismicity rate and their interpretation of the morphology, Escartín *et al.* [2008] concluded that the west flank of the 16.5°N area is one of active detachment faulting.

On the eastern side of the ridge axis at $16^\circ38.4'\text{N}$, a large, basalt-hosted, inactive hydrothermal vent field (Krasnov hydrothermal field, Figure 3) has been the focus of several studies including near-bottom mapping and sampling efforts [e.g., Bel'tenev *et al.*, 2004; Cannat *et al.*, 2013; Cherkashov *et al.*, 2008, 2010; Fouquet *et al.*, 2008]. This hydrothermal field is the largest of the known basalt-hosted sulfide deposits and may contain ≥ 12.8 million tons of sulfide ores [Cherkashev *et al.*, 2013].

Prior to our study and within the immediate vicinity of the 16.5°N area, 11 rock samples had been collected at the ridge axis near $16^\circ18'\text{N}$ and 2 at $16^\circ36'\text{N}$ (PetDb database; <http://www.petdb.org/>) [Dosso *et al.*, 1993]. The samples include fresh looking volcanic rocks and mafic rocks.

3. Data

SeaBeam 3012 multibeam bathymetry data were collected along the track lines shown in Figure 1, which extend 60 km (~ 5 Ma) on each side of the axis. In this paper, we refer to these regional multibeam

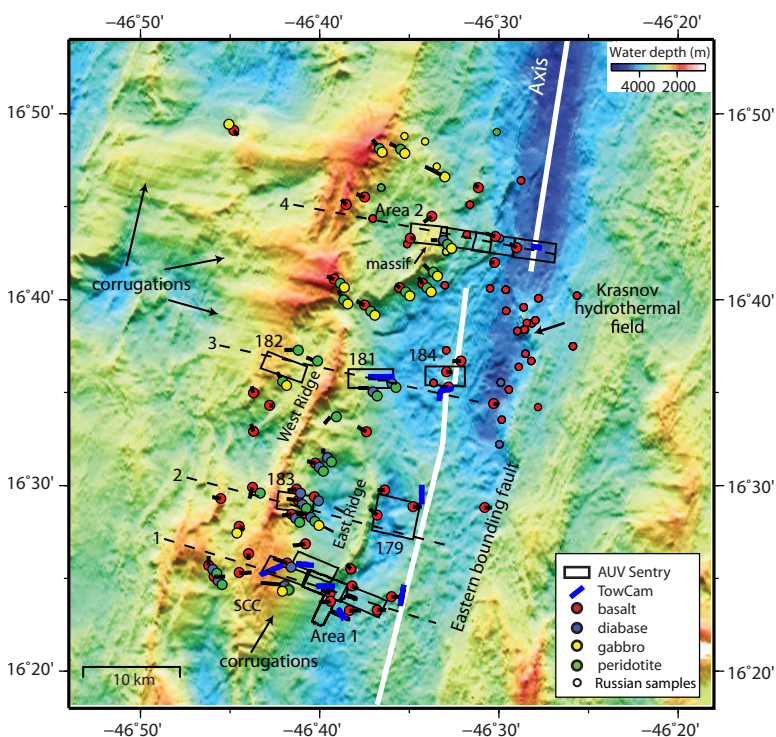


Figure 3. Bathymetric map showing the locations of the *Sentry* surveys, *TowCam* dives, and dredges. Black rectangles: *Sentry* survey areas. Area 1 consists of five *Sentry* surveys and Area 2 consists of four. Numbers identify each of the single surveys. Blue lines: location of nine *TowCam* dives. Short black lines: dredge tracks. Filled circles: color indicates rock lithologies. Small circles: rocks collected during expeditions of the R/V *Professor Logatchev* [Bel'tenev et al., 2006; Cherkashov, personal communication, 2013]. White lines: volcanic axis. Dashed black lines: location of profiles shown in Figure 13. SCC: South Core Complex.

bathymetry data as SeaBeam data, which are shown in Figure 2 with topographic lineations indicated. During the regional survey, a SeaSPY marine magnetometer and a shipboard BG-3 gravimeter collected magnetic and gravity data. Detailed analyses of these data will be completed as part of another study.

AUV *Sentry* surveys were completed over 14 patches of seafloor, each survey mapping an area of about 10 km² (Figure 3). Areas 1 and 2 consist of multiple adjoining dives; single surveys were completed in five other areas. *Sentry* flies ~60–65 m above the seafloor at a speed of ~0.75 kt, and was equipped with the following: (1) Reson 7125 400 kHz multibeam sonar; (2) Edgetech subbottom profiler—CHIRP (4–24 kHz sweep); (3) Edgetech 120/440 kHz side-scan sonar; (4) Seabird 49 Conductivity Temperature Depth (CTD) profiler; (5) Seapoint optical backscatter sensor; (6) Oxidation-reduction potential (ORP) sensor; (7) an electrochemical (Eh) sensor supplied by K. Nakamura; (8) digital still camera with 1 megapixel resolution; and (9) Dual 3-Axis Honeywell smart digital magnetometers. On-bottom time was typically 17–18 h. Survey boxes were designed to obtain 100% bathymetric coverage except in Box 179 (Figure 3) where we spaced out lines to map a larger section of seafloor. In this box, we obtained 100% coverage with the low-frequency (120 kHz) side-scan sonar and 30% coverage with the multibeam sonar. Short photographic runs (a few 100 m along the seafloor) were completed in Box 179 and the westernmost box of Area 2 to test the capability of the *Sentry* digital camera.

The *TowCam* digital camera system was used to obtain seafloor images during nine dives (Figure 3, thick blue lines), often operating simultaneously with *Sentry*. The *TowCam* sled was on bottom for 2–4 h and towed at ~0.3 kt about 5 m above the seafloor. A total of 14,274 images were collected during the nine dives, each with a resolution of 16 megapixels. Water column data also were collected during the runs using a SBE 25 Sealogger CTD profiler.

Dredging was a large component of the operations and many dredges were completed during *Sentry* surveys. The dredge stations are shown in Figure 3 with dredge tracks indicated by black lines, and rock lithologies indicated by circle fill color. We collected 2855 kg of basalt, diabase, gabbro, and peridotite in 63

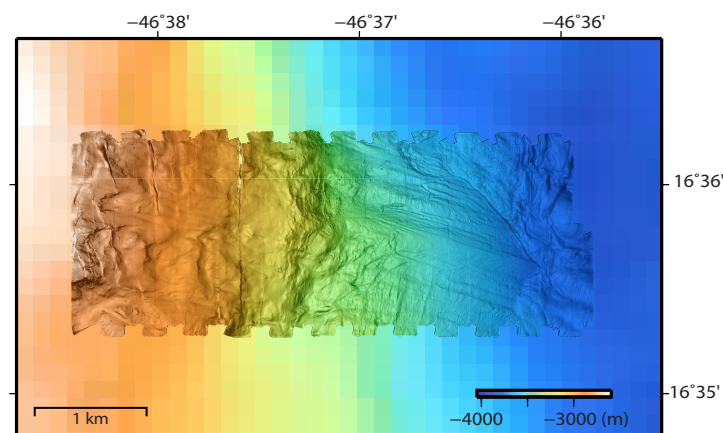


Figure 4. *Sentry* high-resolution bathymetry overlain on SeaBeam bathymetry. The SeaBeam bathymetry data have been gridded at 150 m grid spacing, and the *Sentry* bathymetry at 5 m spacing. The *Sentry* bathymetry data were collected in Box 181 (marked on Figure 3) and reveal details not seen in the regional bathymetry, including corrugations.

successful dredges. In addition, our Russian colleagues provided the locations and types of rocks that they obtained in 2004–2006 during annual cruises of R/V *Professor Logatchev* [Bel'tenev *et al.*, 2006; G. A. Cherkashov, personal communication, 2013]. Small circles on Figure 3 show these locations and their contents. A Miniature Autonomous Plume Recorder (MAPR, <http://www.pmel.noaa.gov/eoi/PlumeStudies/mapr/>) was attached to the dredge wire during the dredge hauls and recorded light-backscattering (for suspended particle concentrations), oxidation-reduction potential (for detecting the presence of reduced chemical species such as H_2S and Fe^{2+}), temperature, and pressure.

This paper focuses on the morphological interpretation of the SeaBeam bathymetry data and the *Sentry* bathymetry and side scan data. The *Sentry* bathymetry data have a horizontal spatial resolution of <1 m compared to the SeaBeam bathymetry data, which have a resolution of 50–100 m. The difference in resolution is illustrated in Figure 4 where *Sentry* bathymetry data from Box 181 (Figure 3) are overlain on our SeaBeam bathymetry. The *Sentry* CHIRP data have been examined by Parnell-Turner *et al.* [2014]. The *Sentry* water column data, and magnetic data, *TowCam* photographs, and dredge samples will be the subjects of separate papers.

concentrations), oxidation-reduction potential (for detecting the presence of reduced chemical species such as H_2S and Fe^{2+}), temperature, and pressure.

4. Large-Scale Characteristics of the Study Area

The 16.5°N study area encompasses two spreading segments [e.g., Thibaud *et al.*, 1998]. Both segments have orientations of $\sim 012^\circ$, which is perpendicular to the calculated spreading direction of $\sim 102^\circ$ [DeMets *et al.*, 2010]. The south segment extends from $16^\circ 18'\text{N}$ to $16^\circ 40.3'\text{N}$, and the north segment extends from $16^\circ 40.6'\text{N}$ to $16^\circ 55'\text{N}$ (Figure 2). The dextral offset between the segments is ~ 6 km. The lines drawn on the bathymetric map in Figure 2 mark topographic lineations and show that both the east and west flanks of the ridge axis have regions of seafloor with features whose orientations are more or less parallel to the current spreading direction. These regions are interpreted as corrugated surfaces, which are typically associated with long-lived detachment faults. The western rift valley wall of the south segment was the main focus of our study.

The southern unit of the valley wall is South Core Complex (SCC on Figure 2, Area 1 on Figure 3), a classic domed, corrugated detachment fault with a slope of $\sim 13^\circ$. The termination where the fault intersects the valley floor is ~ 6.5 km west of the summit of a large AVR that is assumed to be the neovolcanic zone. The corrugations on South Core Complex extend up to near the summit of the massif, and have wavelengths of 400–1600 m and relief of 50–100 m. The nearest breakaway for South Core Complex detachment is at the crest of the massif, which implies that there has been at least 11.5 km of slip on the fault since it broke the seafloor 3.5 km west of the volcanic axis.

The central unit is East Ridge, a 10 km long normal fault that recently developed in front of a section of South Core Complex and West Ridge (Figure 2). We hypothesize that the sections of South Core Complex and West Ridge behind East Ridge became inactive when East Ridge was initiated. The East Ridge fault termination is ~ 3.5 km from the volcanic axis and the fault has an offset of ~ 2.5 km. The outward-facing slope of East Ridge is 20° .

The northern unit is West Ridge, which has an irregular inward-facing slope between 10° and 20° . West Ridge extends along axis for ~ 21 km and at its southern end continues as the crest of South Core Complex. As mentioned above, West Ridge appears to be the breakaway of a flexurally rotated large-offset normal

fault with outward-facing slope of 35° – 40° . Assuming that West Ridge originally broke the valley floor 3.5 km from the volcanic axis, West Ridge fault would have an offset of ~ 7.5 km.

Only the southern section of north segment is included in this study (Area 2, Figure 3). The west wall of the rift valley in Area 2 extends up three normal faults with offsets of <1 km, spaced 2–3 km apart, which end at a small massif with a relief of 800 m (Figure 3). The outward-facing slope of the massif is $\sim 25^{\circ}$ – 30° suggesting that its crest is the breakaway of a long-lived fault. The inward-facing slope is 25° – 35° , has no obvious corrugations, and appears eroded by mass wasting. The breakaway of the massif continues south as a narrow ridge and curves westward to follow the offset between the north and south segments. A notable feature here is that the eastern wall of the axial valley is relatively straight, with little evidence of an offset, composed of what appears to be axis-parallel lineated volcanic terrain.

5. Ridge Axis Morphology

The width of the rift valley floor varies between the south and north segments. The south segment valley floor averages about 10 km wide, while the north segment valley floor is significantly narrower (~ 3 – 4 km in Area 2). An AVR extends along the rift valley floor, the entire length of the south segment (Figure 5a). Its size does not vary systematically along axis; its height ranges from 200 to 400 m and its width from 3 to 5 km. The AVR summit, though, deepens northward and is ~ 500 m deeper in the northern part of the segment (~ 3600 m) than near Area 1 in the south (~ 3100 m). No AVR is present in the north segment where the seafloor is much deeper (~ 4500 m in Area 2).

Sentry surveys were completed over four regions on the valley floor (Figure 5a). *Sentry* bathymetry data from three of these surveys (Area 1, Box 184, and Area 2) are shown in Figures 5b–5d. In Area 1, *Sentry* mapped the western flank of the AVR. Volcanic hummocks dominate the morphology (Figure 5b). Individual hummocks are up to 300 m wide and up to 75 m high, and pile up to form larger features. As an example, the mound of hummocks in the center of the Area 1 swath (Figure 5b) has a relief of ~ 200 m. Faults with relief of 5–20 m and spacing of only a few tens of meters cut the valley floor becoming more pervasive to the west, systematically destroying the volcanic features until they are unrecognizable on the western edge of the survey. Such extensive small-scale faulting is unique to Area 1. *Sentry* Box 184 (Figure 5c) to the north surveyed two overlapping AVRs that are offset by ~ 1 km. Both AVRs are built from individual piled up hummocks. In Area 2, the *Sentry* data show a single relatively unfaulted, cratered, smooth flow ~ 1 km wide and ~ 25 m high, and a pile of hummocks rising up to ~ 100 m immediately to the south. Several hummocky ridges (~ 100 m high) are seen in the western half of the survey. Faults with relief of up to 50 m cut the volcanic morphology. As in Area 1, the degree of faulting increases to the west, but unlike the western edge of the valley floor in Area 1, the volcanic features in Area 2 have not been completely destroyed by 5–20 m high closely spaced faults.

The low-frequency (120 kHz) side-scan sonar data from *Sentry* Box 179 are displayed in Figure 6a. Track spacing during this survey was ~ 600 m, which limited the bathymetric coverage to only 30% of the area (Figure 6b). The survey covered the hanging wall (valley floor) in front of East Ridge where a flexural basin has been created by fault slip. Several constructional volcanic features lie within the basin. A large flat-top flow 1600 m in diameter and 250 m high on its western side extends west from the AVR (Figure 6a); the flow represents ~ 0.5 km³ of lava. Other, smaller flat-top flows are identified, some of which appear to have been fed from the west. Seafloor photographs of the top of the large flat-top flow show sediment covered terrain. The side-scan sonar data indicate that regions on the flank of this large flow have less sediment cover than the top and thus, might represent more recent lava flows or debris fans.

TowCam photographs were obtained within or near each of the *Sentry* surveys at the ridge axis (Figures 5a and 7). Sediment intermingles with pillow lavas in the three camera runs along the AVR in the south segment, and striated pillows were seen in all dives (Figures 7a–7c, TC4, TC5, and TC8). The photographs at the north end of the segment (TC8, Figure 7c) show slightly more sediment on top of the pillows, on average, compared to the two camera runs to the south, although we have not quantified the difference. In Area 2, seafloor photographs of the top of the smooth cratered flow (Figure 7d, TC9) show only flat, sedimented seafloor along the length of the tow.

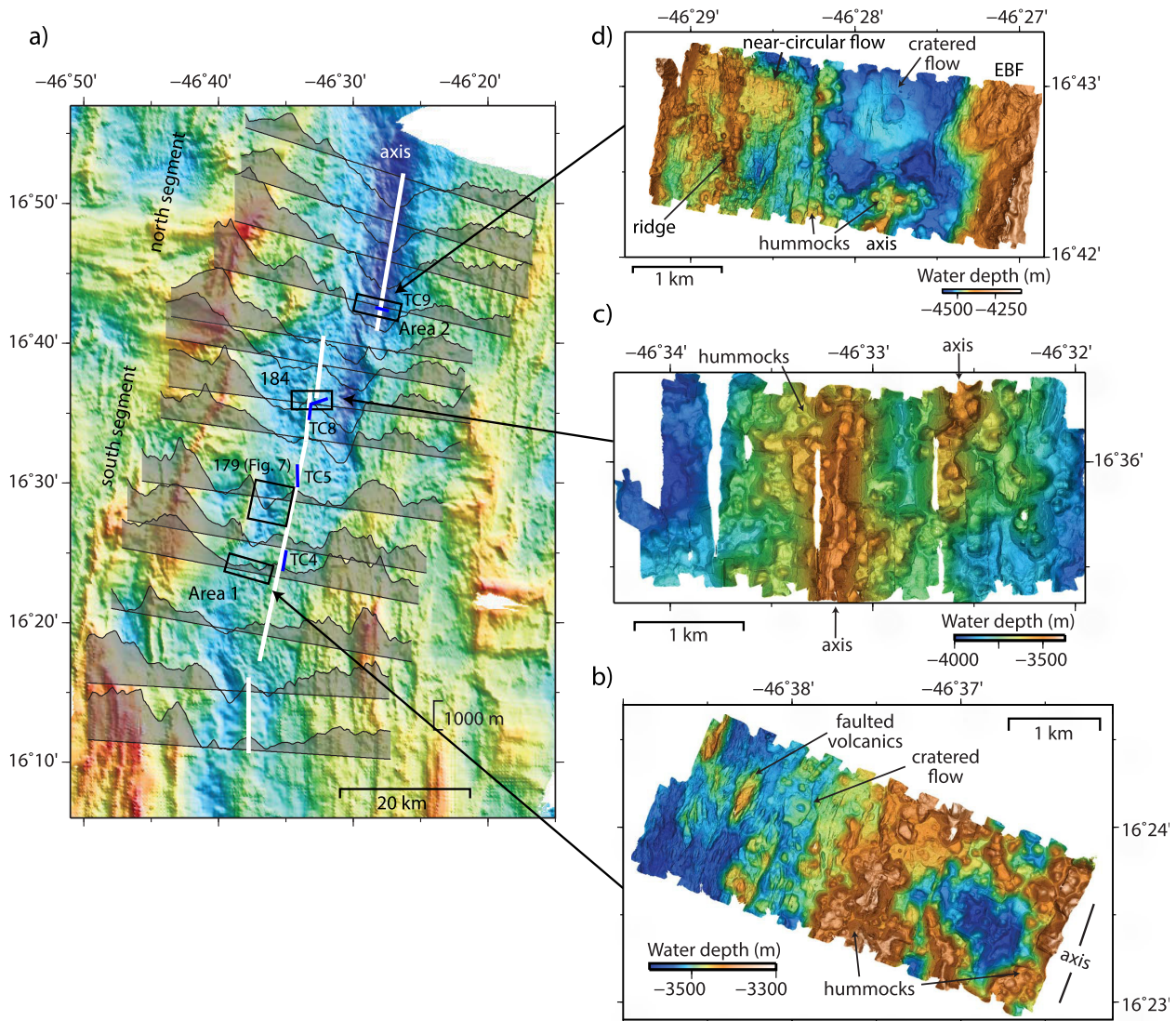


Figure 5. Bathymetry of the ridge axis. (a) SeaBeam bathymetric map with topographic profiles drawn across the axis. Shading on profiles: bathymetry shallower than 3000 m. White lines: ridge axis. Black rectangles: *Sentry* survey locations. Blue lines: *TowCam* (TC) dives labeled by numbers. *Sentry* bathymetric maps of the valley floor are shown for (b) Area 1, (c) Box 184, and (d) Area 2. EBF: eastern boundary fault. Features discussed in the text are labeled.

6. Western Rift Valley Wall

For each of the *Sentry* surveys on the western flank of the ridge axis, the *Sentry* bathymetry data, dredge tracks, rock types sampled, and *TowCam* tracks are shown in Figures 8–12. Slope maps calculated from the *Sentry* bathymetry highlighting the shapes of features, as well as *Sentry* bathymetric profiles, are also shown.

6.1. Area 1

Five adjoining *Sentry* surveys in Area 1 extend from the valley floor onto the corrugated South Core Complex detachment surface to near its crest (Figure 8). The survey includes the southern end of East Ridge and what we interpret as the inactive section of South Core Complex behind East Ridge. The topography at the intersection of East Ridge and South Core Complex is complicated and remains to be understood. Small-scale corrugations run from close to the top of the detachment surface downslope for ~4 km. These corrugations have wavelengths of less than a few hundred meters and amplitudes <10 m. Several outward-facing scarps with relief of <10 m are observed on the corrugated detachment surface. The termination of the detachment surface behind East Ridge is sharp and easily identified. In contrast, the termination of

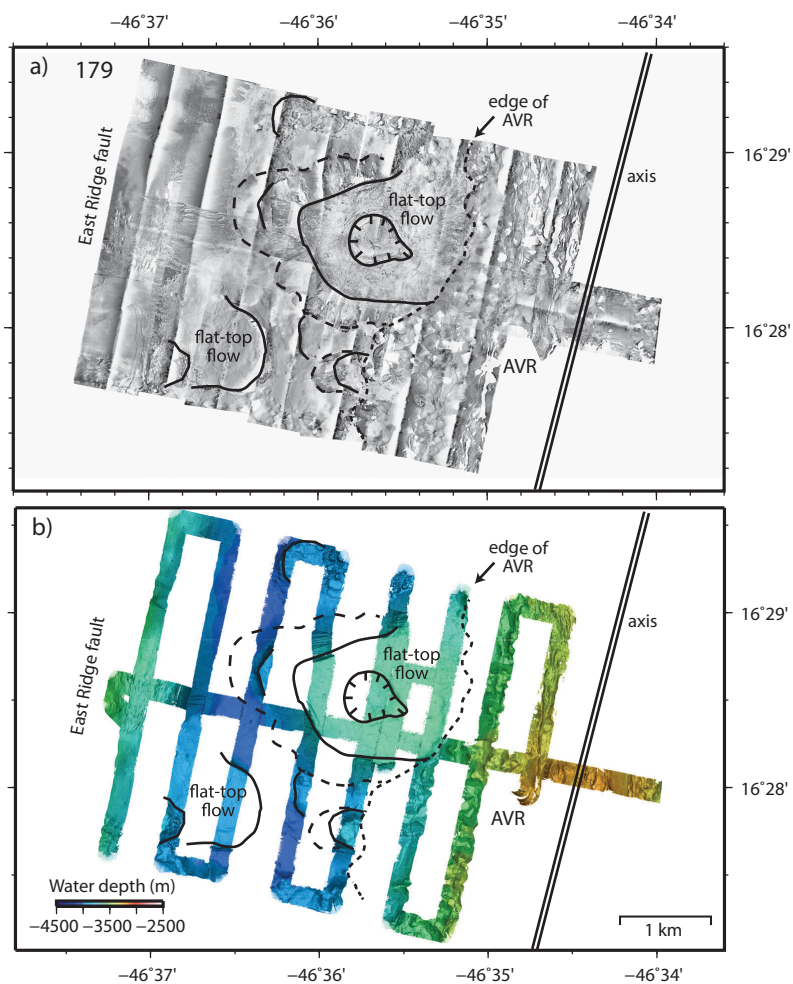


Figure 6. High-resolution data from survey Box 179 (location in Figure 5a). (a) Low-frequency (120 kHz) side-scan sonar data provide 100% coverage of the survey box. Light shades: low reflectivity normally indicative of sediment covered terrain. Dark shades: high reflectivity. (b) Bathymetry data cover only 30% of the survey box. Solid black lines: flat tops of flows. Hachured black line: depression at the top of the large flat-top flow. Long dashed lines: edge of aprons at the base of two of the flows. Short dashed line: edge of the axial volcanic ridge (AVR). Double black line: ridge axis.

South Core Complex with the valley floor is difficult to identify because the western edge of the rift valley is so severely faulted and fissured that it is hard to define where the volcanic morphology begins.

Several dredges completed within and near Area 1 primarily yielded basalt but also diabase, serpentinized peridotite, and gabbro near the top of the massif. Five *TowCam* dives were completed in Area 1. Dive TC4 imaged the AVR as described above (Figure 7a). TC1 was run across the valley floor west of the AVR and the photographs show more extensive sediment cover than along the summit of the AVR. Numerous cracks and faults also are observed on the photographs from TC1 consistent with the observation that deformation of the lavas increases westward from the volcanic axis. TC3 was run over the termination of South Core Complex at the valley floor. Photographs show areas of completely sedimented seafloor, but in the western half of the run there are outcrops that look like slabs of rock that may be the fault surface. Along the eastern half of the run there are regions of basalt rubble, cracks filled with basalt rubble, and what appear to be in situ pillows of the valley floor. The photographs do not pinpoint the location of the fault termination, however. TC2 began near the crest of the massif and ran onto the corrugated surface of South Core Complex. Many of the photographs show sedimented seafloor. Near the top of the massif there are piles of rubble, but it is hard to determine what they represent. Farther along the run, rectangular slabs, some in place, probably represent the fault surface. All of the photographs from TC6 on the section of South Core Complex behind East Ridge show only sedimented seafloor.

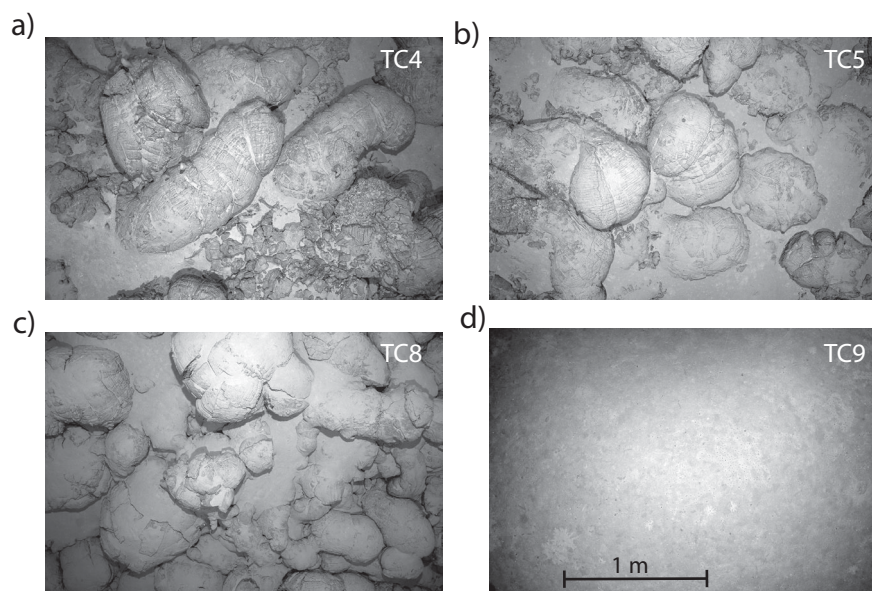


Figure 7. TowCam digital photographs from the ridge axis. TowCam runs are shown in Figure 5a. Sediment and striated pillows are observed in the photographs from (a) TC4 near Area 1, (b) TC5 near Box 179, and (c) TC8 near Box 184. (d) TC9 in Area 2 was run along the top of the smooth cratered flow marked on Figure 5d, and all photographs show sedimented seafloor.

6.2. Area 2

Area 2 (Figure 9) is located north of the right-lateral, nontransform offset between the south and north segments (Figure 3). As described above, there are constructional volcanic features on the valley floor, some with relief of 100 m. The western valley wall consists of four fault blocks. The first three (f1–f3, Figure 9a) have 1 km offsets or less and minor rotations of $<13^\circ$. We infer that these are short-lived faults, each abandoned quickly as the next formed closer to the axis. The top of each fault block is covered by volcanic hummocks and flows similar to those on the valley floor. Dredging on these blocks recovered basalt. A noncorrugated massif is observed west of fault block 3 (f4, Figure 9a). The inward-facing scarp of this massif is significantly modified by mass wasting, producing seafloor slopes of $\sim 30^\circ$. The headwall scars are deeply incised, and blocks a few tens of meters wide and up to 10 m high appear to have fallen down the scarps. A dredge on a headwall scar (Figure 9a) recovered diabase, serpentinized peridotite, and gabbro. The top of this massif is rotated $\sim 25^\circ$ outward (Figure 9b), and seafloor photographs show nearly sediment-free pillow basalts on this slope. Presumably the pillows are swept clean of sediments by currents at the top of the massif. We interpret the massif as a detachment fault with an offset of ~ 4 km.

Between Areas 1 and 2, we surveyed three sections of seafloor in regions of ambiguous topography (Figure 3). Box 181 is at the base of the rift valley wall, and Boxes 182 and 183 are farther off axis. In Boxes 182 and 183, the regional SeaBeam bathymetry data suggest relict corrugations.

6.3. Box 181

Sentry Box 181 is located at the base of the rift valley wall east of West Ridge (Figures 3 and 10). The bathymetry data show a finely corrugated, low-angle detachment fault intersecting the valley floor. The corrugations have wavelengths on the order of only tens of meters and just a few meters of relief (smaller than on the South Core Complex detachment surface, see above). The termination of the detachment fault at its intersection with the volcanic morphology of the valley floor is sharp and located ~ 4.5 km from the volcanic axis. The base of the detachment surface has an average slope of 15° . Its morphology, however, changes significantly upslope. About 1.5 km west of its termination, the detachment surface appears covered by debris, most likely shed from upslope. The seafloor then ramps up for ~ 0.5 km at an average slope of 20° . Farther west, the average slope is 15° , and mass wasting has degraded the fault surface producing small, curved headwall scars with relief <30 m. Corrugations are still visible but less pronounced in this western section of the survey. Numerous outward-facing scarps with relief <15 m have also formed here, similar to those observed on South Core Complex (Figure 8a).

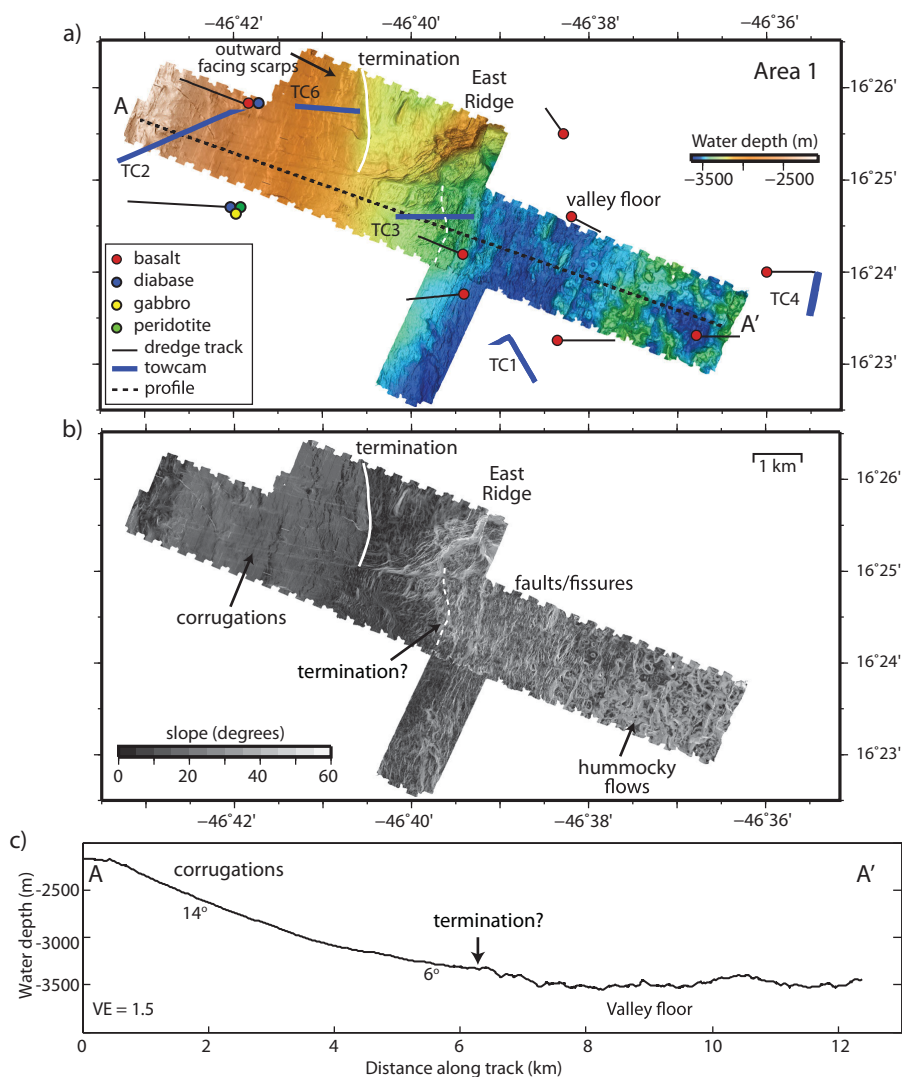


Figure 8. *Sentry* data collected in Area 1 (Figure 3). (a) Bathymetric map. Blue lines: locations of *TowCam* (TC) runs identified by number. Black lines with circles: dredge tracks and rock types indicated by circle fill color. Solid white line: inferred inactive termination of South Core Complex behind East Ridge. Dashed white line: inferred location of the active termination. Dashed black line: location of the bathymetric profile shown in (c). (b) Slope map derived from the *Sentry* bathymetry data for slopes <math><60^\circ</math>. Slopes are calculated for four facing directions (E, W, N, S). Labels as in Figure 8a. (c) Bathymetric profile along the black dashed line in Figure 8a. Seafloor slopes are marked, as well as the inferred location of the fault termination.

Two dredges were made within the region of *Sentry* Box 181 (Figure 10a). One was on the lower corrugated surface and the other was conducted slightly south of the *Sentry* box farther upslope. The two dredges contained diabase, diabase breccia, and serpentinized peridotite.

6.4. Box 182

Box 182 is located behind West Ridge (Figures 3 and 11) where the *SeaBeam* bathymetry data suggest large-scale corrugations (wavelength of several kilometers). The *Sentry* bathymetry data show a landscape profoundly affected by mass wasting. Large sections of the high on the western side of the survey box have collapsed into the depression on the east, leaving large scars. The relief on the headwall scars reaches up to 200 m. Two adjacent semicircular collapses, each nearly 1 km wide, created a spur between them reaching out to the east. It is likely that the spurs are features that we identified previously as corrugations. No volcanic features are observed in this region, and as in the region of mass wasting in Area 2, blocks a few tens of meters wide are scattered over the landscape. Gabbro and serpentinized peridotite were sampled within

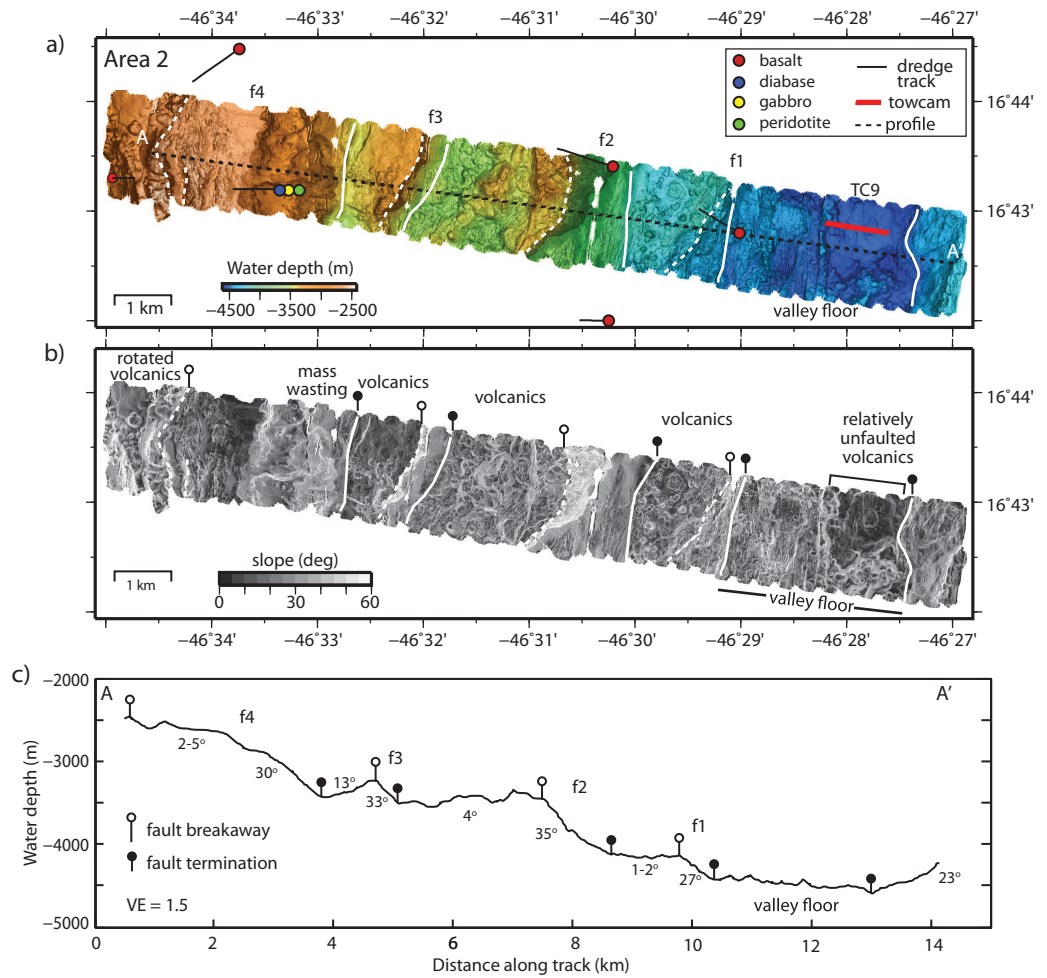


Figure 9. Sentry data collected in Area 2 (Figure 3). (a) Bathymetric map. Red line: location of a TowCam (TC9) run. Black lines with circles: dredge tracks and rock types indicated by circle fill color. f: fault blocks numbered from the axis. Solid white line: fault terminations. Dashed white lines: breakaways of faults. Dashed black line: location of the bathymetric profile in (c). (b) Slope map derived from the Sentry bathymetry for slopes <math>< 60^\circ</math>. Slopes are calculated for four facing directions (E, W, N, S). Vertical lines with open circles: fault breakaways; vertical lines with black filled circles: fault terminations. (c) Bathymetric profile along the black dashed line in Figure 9a. Seafloor slopes are marked as well as fault breakaways and terminations.

and close to this survey area indicating that the seafloor behind West Ridge is a detachment surface that has experienced significant mass wasting as it moved off axis.

6.5. Box 183

Box 183 is located over a section of West Ridge behind East Ridge (Figures 3 and 12). Sentry bathymetry data indicate that this region has experienced mass wasting similar to that in Box 182. A large slump block is marked in Figure 12a. The associated headwall scar is ~1 km wide with a relief of ~100 m. This headwall scar and other scars along the eastern slope of West Ridge have produced large spurs between them, which can be seen in the SeaBeam bathymetry data. Rockslides and a field of large blocks similar to those identified in Area 2 and Box 182 are also seen in the Sentry bathymetry. A number of dredges were completed within and near to Box 183 and yielded basalt, diabase, serpentinized peridotite, and gabbro.

7. Faulting on the Western Flank of the Ridge Axis

To understand the spreading history in the 16.5°N region, we interpret the subsurface faulting along four SeaBeam bathymetric profiles in Figure 13. The profile locations are indicated in Figure 3. Each profile is ~30 km long and modeled following Schouten *et al.* [2010]. The shapes of the faults are based on the flexural fault rotation model of Buck [1988], who showed that as faults continue to slip they rotate outward,

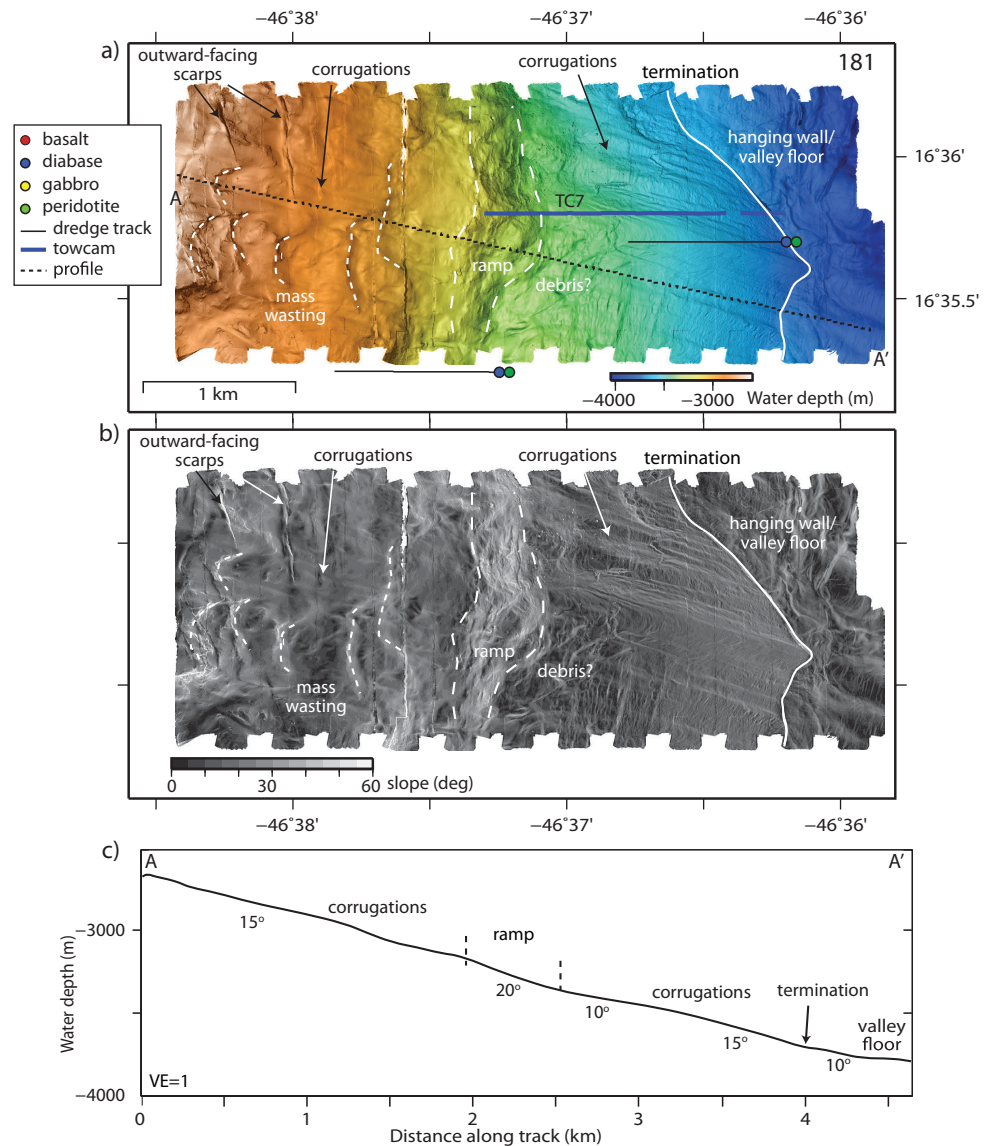


Figure 10. *Sentry* data collected in Box 181 (Figure 3). (a) Bathymetric map. Blue line: location of *TowCam* dive (TC7). Black lines with circles: dredge tracks and rock types indicated by circle fill color. Solid white line: active termination of West Ridge detachment fault. Long-dashed white lines: a section of seafloor that ramps up for ~0.5 km at an average slope of 20°. Short-dashed white lines: headwall scarps from mass wasting of the detachment surface. Corrugations are observed both east and west of the ramp. Black dashed line: location of the bathymetric profile in (c). (b) Slope map derived from the *Sentry* bathymetry for slopes <60°. Slopes are calculated for four facing directions (E, W, N, S). Labels as in Figure 10a. (c) Bathymetric profile along the black dashed line in Figure 10a. Seafloor slopes are marked.

dome upward, and flatten to near horizontal. Long-lived detachment faults may be covered by rafted blocks, which are slices of hanging wall from the valley floor cutoff by normal faults that root in the same primary fault [Buck, 1988]. Rafted blocks are uplifted and rotated with the footwall and carried away from the axis [Reston and Ranero, 2011; Smith et al., 2008]. In most cases, it is difficult to determine from the morphology alone whether a new fault at the axis is a rafted block or whether the older detachment ceased extending and a new detachment developed. Therefore, we present two interpretations for each profile: one of discontinuous faulting and the other of faulting on a single detachment and the formation of rafted blocks.

7.1. Profile 1—South Core Complex

Profile 1 runs from the valley floor through Area 1 and continues west of the crest of South Core Complex. In the discontinuous model (Figure 13a), an older detachment stops slipping and normal two-sided

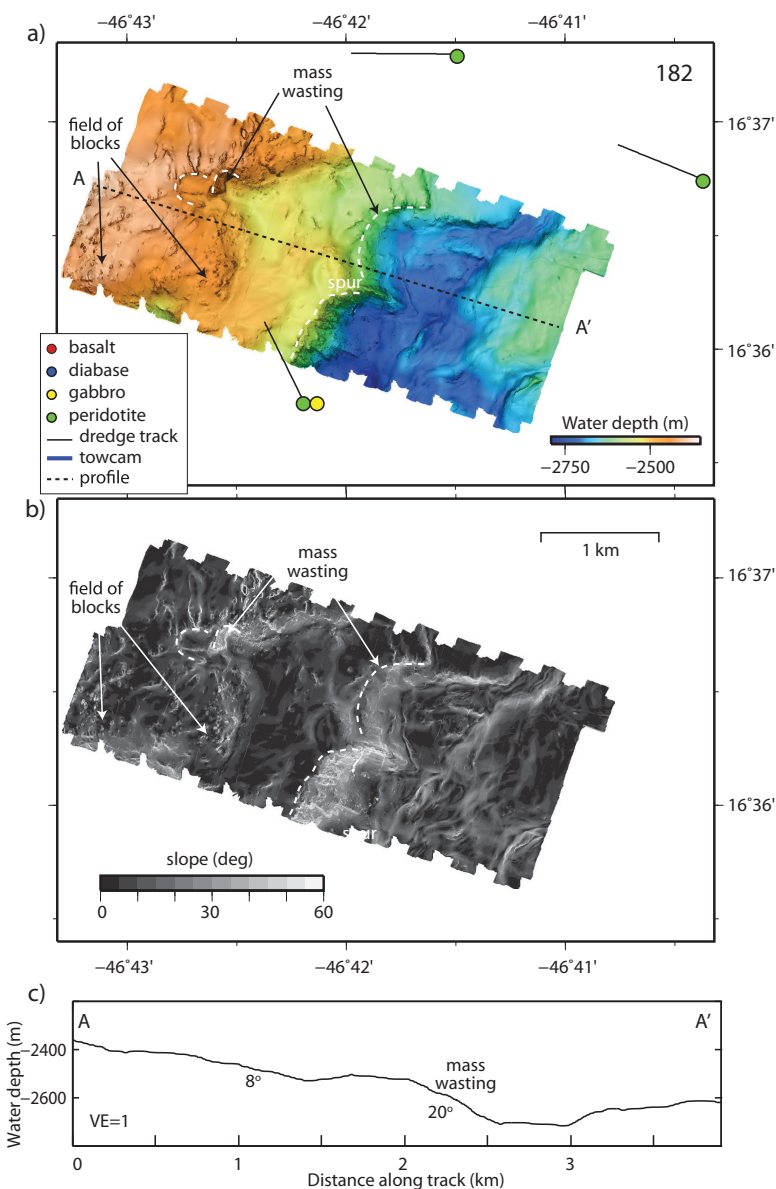


Figure 11. *Sentry* data collected in Box 182 (Figure 3). (a) Bathymetric map. Black lines with circles: dredge tracks and rock types indicated by circle fill color. Dashed white lines: headwall scars from mass wasting of the detachment surface. Fields of large blocks are labeled. Black dashed line: location of the bathymetric profile in (c). (b) Slope map derived from the *Sentry* bathymetry for slopes <math><60^\circ</math>. Slopes are calculated for four facing directions (E, W, N, S). Labels as in Figure 11a. (c) *Sentry* bathymetric profile along the black dashed line in Figure 11a. Seafloor slopes are marked.

magmatic spreading occurs for a few kilometers of half spreading. The breakaway of the new normal fault rotates outward and the detachment surface domes upward as it continues to extend to form South Core Complex. Alternatively, in the continuous model, a single detachment fault has existed for ~ 1.5 Ma, assuming a half-spreading rate of 12.5 km/Ma. The top of South Core Complex is the breakaway of a rafted block that roots into the original detachment surface. Diabase and serpentinized peridotite were dredged west of South Core Complex consistent with the interpretation that a detachment surface is exposed there. Basalt was also dredged in this region and most likely is from the rotated section of valley floor on the outward-facing slope of South Core Complex.

7.2. Profile 2—East Ridge

Profile 2 is ~ 7 km north of Profile 1 (Figure 3), and extends from the volcanic axis, through Box 179, across East Ridge, through Box 183, and across West Ridge (Figure 13b). In the discontinuous model, an earlier

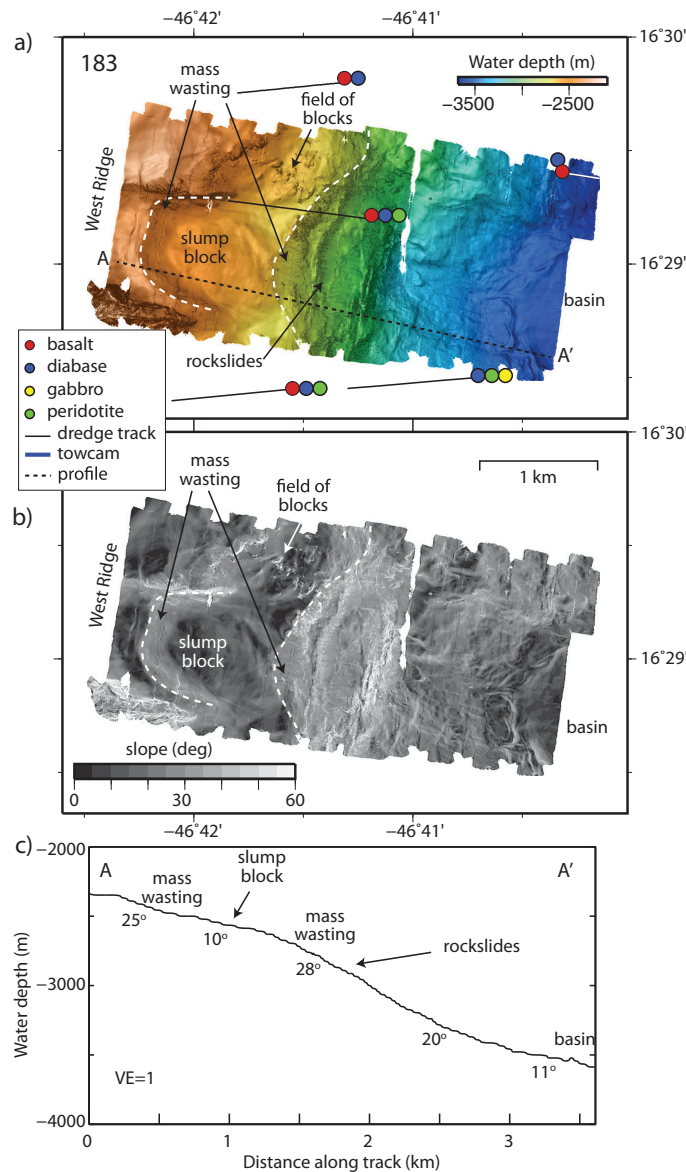


Figure 12. Sentry data collected in Box 183 (Figure 3). (a) Bathymetric map. Black lines with circles: dredge tracks and rock types indicated by circle fill color. Dashed white lines: head-wall scars from mass wasting of the seafloor. Black dashed line: location of the bathymetric profile in (c). A field of blocks and the location of rockslides are labeled. (b) Slope map derived from the Sentry bathymetry for slopes $<60^\circ$. Slopes are calculated for four facing directions (E, W, N, S). Labels as in Figure 12a. (c) Bathymetric profile along the black dashed line in Figure 12a. Seafloor slopes are indicated.

detachment fault stops slipping. After a period of normal magmatic spreading, West Ridge detachment forms. It too stops slipping and normal two-sided magmatic spreading occurs for several km before East Ridge fault forms. In the continuous model, both West Ridge and East Ridge are rafted blocks on a single detachment that has existed for at least 1.7 Ma.

7.3. Profile 3—West Ridge

Profile 3 is ~ 12 km north of Profile 2 and runs across the valley floor near to Box 184, through Box 181, and extends westward close to Box 182 (Figure 13c). In the discontinuous model, an older detachment stops slipping and normal two-sided magmatic spreading occurs for a short period. West Ridge fault forms next, rotating outward as it slips. The section of magmatic crust created during the period between faulting is rafted up the rift valley wall. In this interpretation, it is possible that the ramp identified in Box 181 (Figure 10) marks the base of crustal material.

In a continuous faulting model, West Ridge fault bounds a rafted block. In this interpretation, the original detachment fault has been slipping for at least 1.7 Ma. If West Ridge is a rafted block, it is possible that the ramp, instead of marking the base of

the crust as in the discontinuous model, may mark the deep tip of the rafted block lying on the original detachment surface.

7.4. Profile 4—North Segment

Profile 4 runs through Area 2 in the north segment (Figure 13d). In the discontinuous model, an earlier detachment fault stops slipping and two-sided magmatic spreading occurs. A new detachment fault initiates and forms the small massif on the western edge of Area 2. This detachment has an offset of ~ 4 km; it stops slipping at ~ 0.3 Ma after which three successive short-lived faults form. In a continuous faulting model, the massif is a rafted block that roots into an older detachment fault that has been slipping for at least 1.7 Ma. As in the discontinuous model, however, the Area 2 detachment fault stops slipping at ~ 0.3 Ma, and three short-offset faults form.

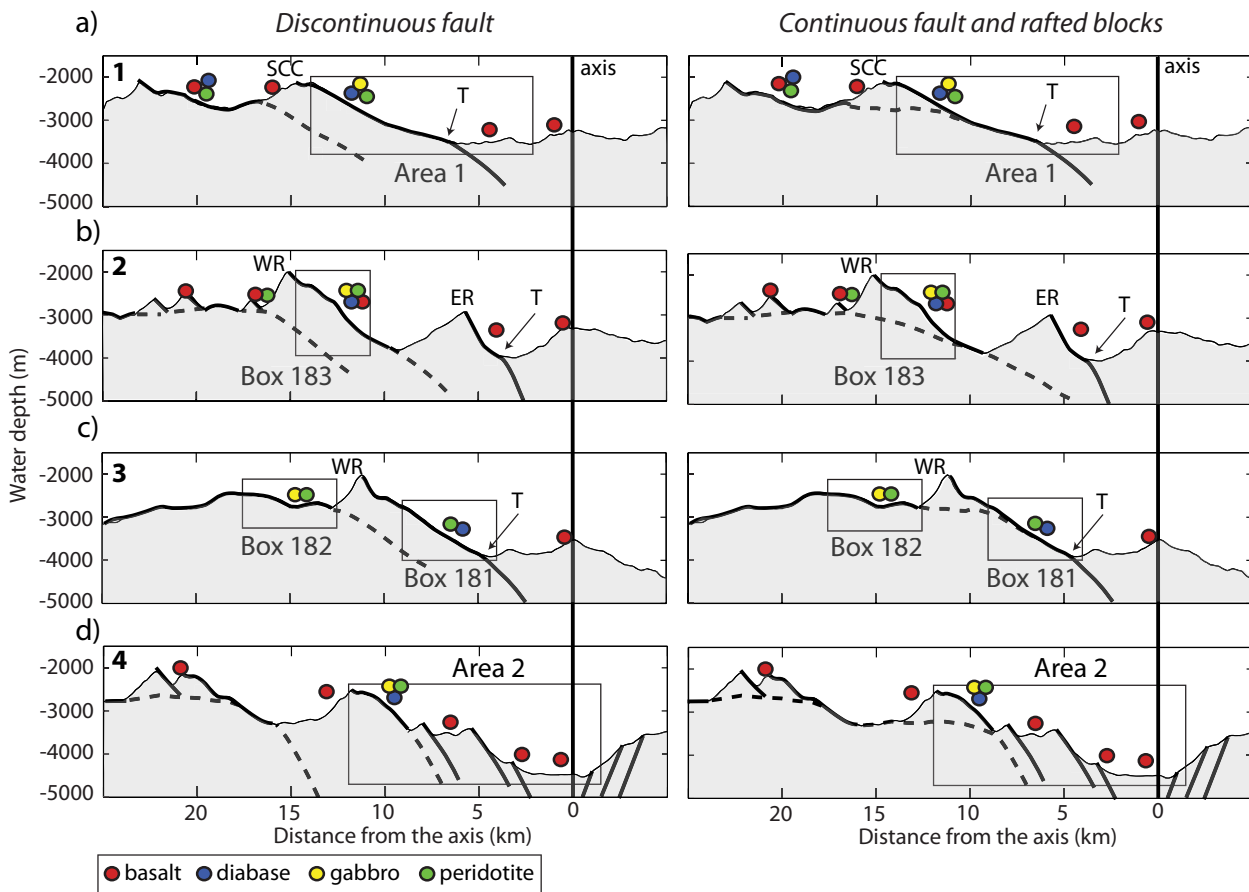


Figure 13. Subsurface interpretation of faulting along four SeaBeam profiles. The profile locations are shown in Figure 3. (a) Profile 1—Area 1, (b) Profile 2—East Ridge, (c) Profile 3—West Ridge, and (d) Profile 4—Area 2. Two models for detachment fault formation are presented for each profile. In the discontinuous model, faulting ceases on an older detachment fault, and after a period of normal magmatic spreading a new detachment fault forms. In the continuous model, new normal faults at the axis root into the single, main detachment, and a section of valley floor is transferred from the hanging wall to the footwall as a rafted block. Boxes: locations along the profiles of the *Sentry* surveys. Bold black line: fault surface. Black dashed line: subsurface extent of a detachment fault. Black vertical line: ridge axis. T: termination.

8. Discussion

8.1. Detachment Fault Morphologies at 16.5°N

At the slow spreading MAR, oceanic detachment faults exhibit several morphologies in the regional bathymetry data. The classic domed, corrugated detachment fault surfaces are easily recognizable, and lower crustal and upper mantle rocks have been drilled and sampled from many of them [Blackman *et al.*, 2006; Cann *et al.*, 1997; Dick *et al.*, 2008; Tucholke *et al.*, 1998]. Noncorrugated massifs from which lower crustal and upper mantle rocks have been obtained are also interpreted as detachment faults [e.g., Dick *et al.*, 1981]. Examples of noncorrugated massifs include the TAG massif at 26°N, associated with a steeply dipping zone of earthquakes reaching 7 km below the spreading axis, apparently marking the subsurface detachment fault [deMartin *et al.*, 2007], and several massifs in the region south of the Fifteen-Twenty fracture zone [Schroeder *et al.*, 2007] including Logatchev at 14°45'N [Cherkashov *et al.*, 2010]. Finally, narrow linear ridges that are formed as the breakaway of long-lived faults rotate outward are important indicators of detachment faulting [MacLeod *et al.*, 2009; Smith *et al.*, 2008]. In our survey area, South Core Complex is a classic corrugated detachment surface. The detachment fault at the western edge of Area 2 is an example of a noncorrugated massif. East and West Ridges are back-tilted ridges marking fault breakaways.

The *Sentry* survey within Box 181 (Figure 10) revealed a new detachment fault morphology. The irregular, low-angle rift valley wall seen in the SeaBeam bathymetry is in fact, a finely corrugated detachment fault surface with a sharp termination at the valley floor. The corrugations have a wavelength of tens of meters and relief of a few meters. Fine-scale corrugations have been observed previously on detachment surfaces

[Blackman *et al.*, 2002; MacLeod *et al.*, 2002, 2009; Mallows and Searle, 2012], but only on those surfaces that also have larger-scale corrugations. Thus, it is likely that some of the other areas along the MAR previously interpreted as low-angle and irregular surfaces may in fact be long-lived detachment surfaces with exposures of finely corrugated fault surfaces.

As described in the previous section, rafted blocks are sections of hanging wall (valley floor) cutoff by normal faults that root into a primary detachment fault. As they are carried off axis, rafted blocks are uplifted and rotated with the detachment footwall. Rafted blocks have been imaged seismically on older Atlantic seafloor crust [Reston and Ranero, 2011], and their formation is probably common in the oceans. Reston and Ranero [2011] suggested that it may be difficult to recognize the morphology of detachment faulting in those areas where the exhumed detachment surface is covered by rafted blocks. As shown here and in previous studies, the breakaways of rafted blocks rotate outward to form narrow ridges that are similar to the ridges that mark the rotated breakaways of new long-lived faults [Schouten *et al.*, 2010; Smith *et al.*, 2008]. Thus areas of detachment faulting will still be recognizable by the large outward rotation ($>25^\circ$) of the fault blocks. As shown in Figure 13, however determining whether a narrow ridge marks the breakaway of a rafted block or that of a new detachment fault from the morphology alone is difficult.

8.2. Axial Processes

The outward rotation of normal faults with increasing extension, from small offset faults to long-lived detachments, has been described using models of fault flexure [e.g., Buck, 1988]. Such models require an estimate of the effective elastic thickness of the axial lithosphere, Te , which specifies the flexural wavelength. The west face of East Ridge dips 20° . Assuming this outward-facing slope is due to the flexural rotation of an originally subhorizontal section of the rift valley floor, this implies 20° of outward rotation which for a 2.5 km offset indicates a $Te = 0.5\text{--}1$ km [Smith *et al.*, 2008, Figure 6]. This value of Te is similar to the values found at the 13°N detachment faults [Smith *et al.*, 2008] and several central North Atlantic detachment faults [Schouten *et al.*, 2010].

A clearly identifiable AVR exists along the length of the south segment adjacent to South Core Complex, East Ridge, and West Ridge. The AVR is several hundred meters high and a few kilometers wide, consistent with the sizes of AVRs described at other sections of the MAR [e.g., Searle *et al.*, 2010; Smith and Cann, 1993]. Because modeling suggests that detachment faults form primarily when the fraction of plate separation (M) taken up by magma accretion is between ~ 0.3 and 0.5 [Buck *et al.*, 2005; Olive *et al.*, 2010; Tucholke *et al.*, 2008], we infer that M is at the high end of this range in areas with detachment morphology and robust AVRs. An M of 0.5 would imply that 50% of the extension is taken up by detachment faulting and 50% by magmatic accretion (which includes minor faulting).

No AVR is present in Area 2 where water depths average ~ 4500 m (compared to ~ 3400 m adjacent to South Core Complex). We interpret Area 2 as having lower magma supply and an $M \ll 0.5$. It is impossible to have a better estimate of M , but since only short-offset normal faults have formed in Area 2 for the last ~ 0.3 Ma, the true relationship between magma supply and faulting style probably is not simple.

The distances of fault terminations from the volcanic axis vary along the axis in our study area. At South Core Complex, the location of the fault termination is not known precisely, but the data suggest it is ~ 6.5 km from the volcanic axis. At West Ridge (Sentry Box 181), which has slipped for a similar length of time as South Core Complex, the termination is ~ 4.5 km from the volcanic axis. The location of a fault termination may be controlled by the amount of volcanic infill covering a sloping detachment surface. Thus, because of the large volume of infill adjacent to South Core Complex, lavas cover more of the detachment surface and its termination is far from the volcanic axis while at West Ridge where the volume of volcanic infill is not as large, the termination is closer to the axis. Note that in Area 1 where volcanic infill is large, the valley floor lavas near to the termination are significantly faulted and fissured. The low angle of the emerging detachment footwall (6°) in this region may enhance deformation of the thin wedge of hanging wall lavas covering it, leading to the more intense faulting and fissuring observed in this area.

8.3. Evolution of Detachment Surfaces

Except at South Core Complex, we observe significant mass wasting of detachment surfaces as they move off axis. Where mass wasting is substantial, spurs have formed between large semicircular headwall scars (see Box 183, Figure 11). The spurs are elongate in a direction close to the slip direction, and large enough to be seen in

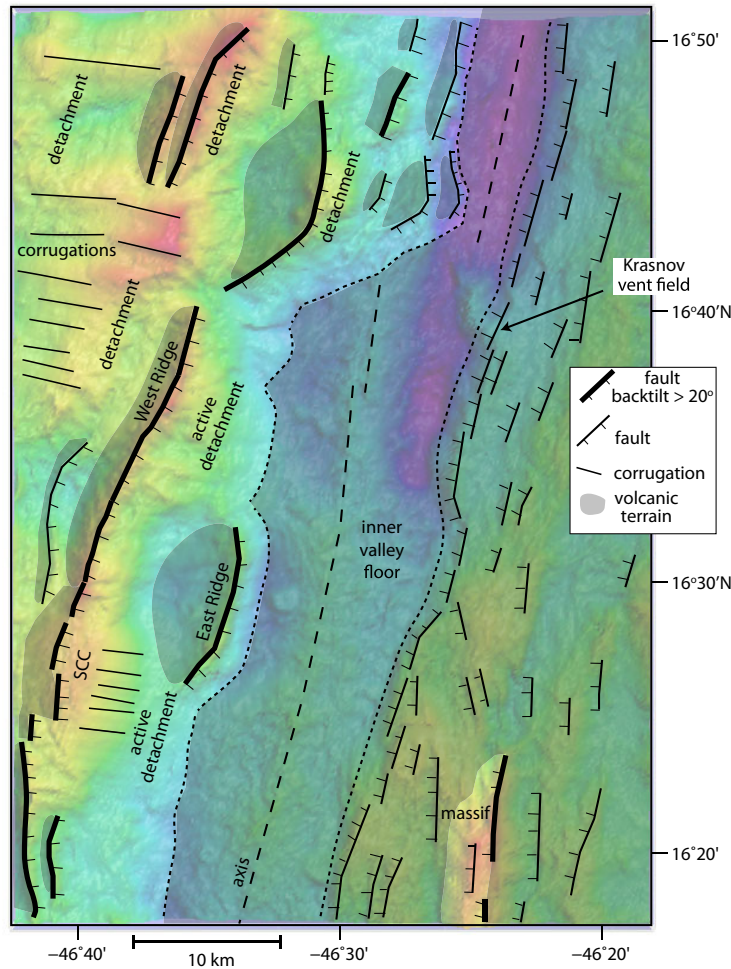


Figure 14. Interpretation of faulting at the 16.5° region of the MAR. The bathymetry data are shown beneath the interpretation. Long dashed lines: volcanic axis. Short dashed lines: edge of the inner valley floor. Thin hachured black lines: breakaways of faults. Bold hachured black lines: breakaways of faults with outward rotation > 20°. Darker shading: volcanic seafloor. The western flank of the study area is composed primarily of active and extinct detachment surfaces. A noncorrugated massif with outward-facing slope of >20° is present on the eastern flank and may be a detachment fault.

Complex and West Ridge from the *Sentry* data (~10–100 m, ~5 m) and centimeter-scale striations [e.g., *Karson, 1999*]. On most detachment surfaces, corrugations coexist on a wide range of scales [*Blackman et al., 2002; MacLeod et al., 2002, 2009; Mallows and Searle, 2012*], superimposed one on the other. How do corrugations form?

Tucholke et al. [2008] suggested that at mid-ocean ridges with low melt supply the uneven distribution of magmatic intrusions beneath the ridge axis creates an irregular brittle-ductile transition. As a detachment extends in such a region, the footwall takes on the shape of the base of the brittle layer exhuming large-scale megamullions. This is analogous to the geologic continuous casting model of *Spencer* [1999]. We do not think, however, that the irregularity in magma distribution at the axis could offer a mechanism for the formation of all corrugations. It is possible that some corrugations, especially those observed above the brittle/ductile transition close to the fault breakaway at West Ridge and South Core Complex, may be formed from segmented fault traces that break through and connect (anastomosing faults) [*Ferrill et al., 1999; Wong and Gans, 2008*]. Such corrugations continue to be formed as the detachment slips. Of note is that in both areas the corrugations close to the breakaway appear to be continuous with the corrugations close to the termination.

8.5. Faulting at 16.5°N

In the 16.5°N region, lineations that parallel the slip direction and are continuous for up to 10 km are observed on the western flank of the axis. We interpret these lineations as large-scale corrugations formed

the regional bathymetry. Their formation may be controlled by preexisting large-scale corrugations that have the same wavelength of a few kilometers.

Outward-facing scarps with relief of <15 m are seen on the *Sentry* bathymetry data collected over the corrugated surfaces of South Core Complex and West Ridge detachment. The origin of these faults is unknown, but a possibility is that they form as the detachment surface flexes and rotates outward to near horizontal. Another possibility is that they form from spalling or flaking of the fault surface once it is exhumed [e.g., *Petit, 1987*].

8.4. Controls on the Formation of Corrugations

Corrugations have been observed at many scales, from megamullions (wavelength of ~10 km and amplitude of ~500 m) [*Tucholke et al., 1998*] through corrugations (~1 km, ~50–100 m) to small-scale features such as the corrugations described on South Core

during slip on long-lived detachment faults. The lineations indicate that detachment faulting has dominated parts of the western flank of the 16.5°N region for perhaps as long as 5 Ma (Figure 2), assuming symmetrical spreading. Nearer to the axis, we extend our findings from the *Sentry* surveys and our interpretation of subsurface faulting to identify the key tectonic features.

Figure 14 summarizes our findings. The breakaways of South Core Complex, West Ridge and the Area 2 massif are 12–15 km from the current axis, suggesting that they were all active at the same time (~0.7–0.9 Ma assuming they initiated 3.5 km from the volcanic axis and a half-spreading rate of 12.5 km). These features may have linked together to form a single detachment along ~50 km of the axis. Detachment faulting stopped in Area 2, with the initiation of a sequence of short-lived faults. The breakaway of the earliest short-lived fault is ~7.5 km from the axis suggesting that it formed ~0.3 Ma. Farther south the 10 km long East Ridge fault formed at ~0.2 Ma (given its 2.5 km offset), and interrupted the slip on the detachment surface behind it. From the data in hand, we cannot determine whether East Ridge is a rafted block or a new fault that formed after a period of two-sided magmatic spreading (Figure 13). The curved shape of the north and south tips of East Ridge, however, suggests that it could be breaking through to connect to what might be a single segment-long detachment surface.

There are presently no active detachment faults on the eastern side of the ridge axis along the south and north segments. The SeaBeam bathymetry data show, however, that detachment fault morphologies are present over a large portion of the eastern flank on crust > 2 Ma (Figure 2). The presence of these features on off-axis seafloor east of the axis, in combination with the detachment morphologies that are observed west of West Ridge, implies that within the last 5 Ma both sides of the axis have experienced detachment faulting perhaps even simultaneously.

9. Conclusions

Detachment faulting has dominated parts of the western flank of the 16.5°N region for perhaps as long as 5 Ma. Active detachment faulting currently is limited to the western side of the axis. Nonetheless, detachment fault morphologies also are present over a large portion of the eastern flank on crust >~2 Ma indicating that within the last 5 Ma parts of the ridge axis may have experienced periods of two-sided detachment faulting.

The study area exhibits a variety of morphologies indicative of detachment faulting including a classic corrugated massif, noncorrugated massifs, and back-tilted narrow ridges marking detachment fault breakaways. We also recognize a new morphology: a low-angle (10°–20°), irregular surface in the regional bathymetry is shown to be a corrugated detachment surface. These corrugations have wavelengths of only tens of meters and amplitudes of a few meters and are only visible in the high-resolution *Sentry* bathymetry.

Multiscale corrugations extend from the termination of detachment fault surfaces to only a few kilometers from the fault breakaway. The presence of corrugations that close to the breakaway of the detachment faults suggests that some corrugations form above the brittle/ductile transition perhaps by anastomosing faults.

A robust AVR, several hundred meters high and a few kilometers wide, exists along the 40 km length of the south segment adjacent to active detachments faults. We infer that $M = 0.5$ in this segment (the fraction of plate separation accommodated by magma accretion) [Buck *et al.*, 2005; Olive *et al.*, 2010; Tucholke *et al.*, 2008]. In the north segment where water depths reach ~4500 m and no AVR is present, we conclude that magma supply is lower and thus $M \ll 0.5$. Currently, active detachment faulting does not appear to occur in the north segment. These observations add to the growing evidence that detachment faulting is likely dependent on a balance between several factors including magma input.

References

- Baines, A. G., M. J. Cheadle, B. E. John, and J. J. Schwartz (2008), The rate of oceanic detachment faulting at Atlantis Bank, SW Indian Ridge, *Earth Planet. Sci. Lett.*, 273(1-2), 105–114.
- Bel'tenev, V., A. Shagin, V. Markov, I. Rozhdestvenskaya, T. Stepanova, G. Cherkashev, I. Fedorov, A. Rummyantsev, and I. Poroshina (2004), A new hydrothermal field at 16°38.4'N, 46°28.5'W on the Mid-Atlantic Ridge, *InterRidge News*, 13, 5–6.
- Bel'tenev, V. E., A. A. Shagin, V. F. Markov, I. I. Rozhdestvenskaya, L. I. Lazareva, I. P. Fedorov, G. A. Cherkashev, T. V. Stepanova, I. M. Poroshina, and V. V. Shilov (2006), New hydrothermal ore field at 16°38' N of the Mid-Atlantic Ridge, *Doklady Earth Sci.*, 408(1), 530–534.

Acknowledgments

The SeaBeam bathymetry data in this paper are publicly available at the National Geophysical Data Center (NGDC). The *Sentry* data are held on a National Deep Submergence Server (NDSF) server at Woods Hole Oceanographic Institution and are available on request. The data from the dredges can be accessed on the Petrological Database website (PetDB). The bathymetry and side scan data were edited, combined, and gridded using MB-system [Caress and Chayes, 1996], and displayed using the Generic Mapping Tools (GMT) software [Wessel and Smith, 1991]. This work was supported by the National Science Foundation grant OCE-1155650. We thank the captain and crew of the R/V *Knorr* for their help and enthusiasm during our cruise. We also thank the *Sentry* group who worked hard to complete 14 *Sentry* dives over the challenging topography of the MAR. L. Christiansen, D. Fornari, and M. Swartz worked tirelessly during the *TowCam* runs. G. Cherkashov graciously provided us with the locations and types of rocks sampled in the 16.5°N area. We had several fruitful discussions with D. Fornari, B. Tucholke, and J. Escartín. We also thank two anonymous reviewers for their constructive comments.

- Blackman, D. K., et al. (2002), Geology of the Atlantis Massif (Mid-Atlantic Ridge, 30°N): Implications for the evolution of an ultramafic oceanic core complex, *Mar. Geophys. Res.*, **23**, 443–469.
- Blackman, D. K., B. E. Ildefonse, B. E. John, Y. Ohara, D. J. Miller, C. J. MacLeod, and Expedition 304/305 Scientists (2006), Oceanic core complex formation, Atlantis Massif, *Proceedings of Integrated Ocean Drilling Program, 304/305*, 304, 605 pp., Ocean Drill. Program, College Station, Tex., doi:10.2204/iodp.proc.304305.2006.
- Buck, W. R. (1988), Flexural rotation of normal faults, *Tectonics*, **7**(5), 959–973.
- Buck, W. R., L. L. Lavie and A. N. B. Poliakov (2005), Modes of faulting at mid-ocean ridges, *Nature*, **434**, 719–723.
- Cann, J. R., D. K. Blackman, D. K. Smith, E. McAllister, B. Janssen, S. Mello, E. Avgerinos, A. R. Pascoe, and J. Escartin (1997), Corrugated slip surfaces formed at North Atlantic ridge-transform intersections, *Nature*, **385**, 329–332.
- Cannat, M., et al. (1995), Thin crust, ultramafic exposures, and rugged faulting patterns at the Mid-Atlantic Ridge (22°–24°N), *Geology*, **23**, 49–52.
- Cannat, M., D. Sauter, V. Mendel, E. Ruellan, K. Okino, J. Escartin, V. Combiere, and M. Baala (2006), Modes of seafloor generation at a melt-poor ultraslow-spreading ridge, *Geology*, **34**(7), 605–608.
- Cannat, M., A. Mangeny, H. Ondreas, Y. Fouquet, and A. Normand (2013), High-resolution bathymetry reveals contrasting landslide activity shaping the walls of the Mid-Atlantic Ridge axial valley, *Geochem. Geophys. Geosyst.*, **14**, 998–1011, doi:10.1002/ggge.20056.
- Caress, D. W., and D. N. Chayes (1996), Improved processing of Hydrosweep DS multibeam data on the R/V Maurice Ewing, *Mar. Geophys. Res.*, **18**, 631–650.
- Cherkashev, G. A., et al. (2013), Massive sulfide ores of the northern equatorial Mid-Atlantic Ridge, *Oceanology*, **53**(5), 607–619.
- Cherkashov, G., V. Bel'tenev, V. Ivanov, L. Lasareva, M. Samovarov, V. Shilov, T. Stepanova, G. P. Glasby, and V. Kuznetsov (2008), Two new hydrothermal fields at the Mid-Atlantic Ridge, *Mar. Georesour. Geotechnol.*, **26**, 308–316.
- Cherkashov, G., et al. (2010), Seafloor massive sulfides from the northern equatorial Mid-Atlantic Ridge: New discoveries and perspectives, *Mar. Georesour. Geotechnol.*, **28**, 222–239.
- deMartin, B. J., R. A. Reves-Sohn, J. P. Canales, and S. E. Humphris (2007), Kinematics and geometry of active detachment faulting beneath the TAG hydrothermal field on the Mid-Atlantic Ridge, *Geology*, **35**(8), 711–714. [Available at <http://geology.gsapubs.org/content/35/8/711.short>.]
- DeMets, C., R. G. Gordon, and D. F. Argus (2010), Geologically current plate motions, *Geophys. J. Int.*, **181**, 1–80.
- Dick, H. J. B., G. Thompson, and W. B. Bryan (1981), Low angle faulting and steady-state emplacement of plutonic rocks at ridge-transform intersections (abstract), *EOS Trans. AGU*, **62**, 406.
- Dick, H. J. B., J. Lin, and H. Schouten (2003), An ultraslow-spreading class of ocean ridge, *Nature*, **426**, 405–412.
- Dick, H. J. B., M. A. Tivey, and B. E. Tucholke (2008), Plutonic foundation of a slow-spreading ridge segment: Oceanic core complex at Kane Megamullion, 23°30'N, 45°20'W, *Geochem. Geophys. Geosyst.*, **9**, Q05014, doi:10.1029/2007GC001645.
- Dosso, L., H. Bougault, and J.-L. Joron (1993), Geochemical morphology of the North Mid-Atlantic Ridge, 10°–24°N: Trace element-isotope complementarity, *Earth Planet. Sci. Lett.*, **120**, 443–462.
- Escartin, J., D. K. Smith, J. Cann, H. Schouten, C. H. Langmuir, and S. Escrig (2008), Central role of detachment faults in accretion of slow-spread oceanic lithosphere, *Nature*, **455**, 790–794, doi:10.1038/nature07333.
- Ferrill, D. A., J. A. Stamatakos, and D. Sims (1999), Normal fault corrugation: Implications for growth and seismicity of active normal faults, *J. Struct. Geol.*, **21**(8–9), 1027–1038.
- Fouquet, Y., et al. (2008), Serpentine cruise—Ultramafic hosted hydrothermal deposits on the Mid-Atlantic Ridge: First submersible studies on Ashadze 1 and 2, Logatchev 2 and Krasnov vent fields, *InterRidge News*, **17**, 16–21.
- Grimes, C. B., B. E. John, M. J. Cheadle, and J. L. Wooden (2008), Protracted construction of gabbroic crust at a slow spreading ridge: Constraints from 206Pb/238U zircon ages from Atlantis Massif and IODP Hole U1309D (30°N, MAR), *Geochem. Geophys. Geosyst.*, **9**, Q08012, doi:10.1029/2008GC002063.
- Karson, J. A. (1999), Geological investigation of a lineated massif at the Kane Transform Fault: Implications for oceanic core complexes, *Philos. Trans. R. Soc. London A*, **357**, 713–740.
- MacLeod, C. J., et al. (2002), Direct geological evidence for oceanic detachment faulting: The Mid-Atlantic Ridge, 15°45'N, *Geology*, **30**(10), 279–282.
- MacLeod, C. J., R. C. Searle, B. J. Murton, J. F. Casey, C. Mallows, S. C. Unsworth, K. L. Achenbach, and M. Harris (2009), Life cycle of oceanic core complexes, *Earth Planet. Sci. Lett.*, **287**, 333–344.
- Mallows, C., and R. C. Searle (2012), A geophysical study of oceanic core complexes and surrounding terrain, Mid-Atlantic Ridge 13°N–14°N, *Geochem. Geophys. Geosyst.*, **13**, Q0AG08, doi:10.1029/2012GC004075.
- Ohara, Y., T. Yoshida, and S. Kasuga (2001), Giant megamullion in the Perece Vela Backarc basin, *Mar. Geophys. Res.*, **22**, 47–61.
- Okino, K., K. Matsuda, D. Christie, Y. Nogi, and K. Koizumi (2004), Development of oceanic detachment and asymmetric spreading at the Australian-Antarctic Discordance, *Geochem. Geophys. Geosyst.*, **5**, Q12012, doi:10.1029/2004GC000793.
- Olive, J.-A., M. D. Behn, and B. E. Tucholke (2010), The structure of oceanic core complexes controlled by the depth distribution of magma emplacement, *Nat. Geosci.*, **3**, 491–495, doi:10.1038/ngeo888.
- Parnell-Turner, R., J. R. Cann, D. K. Smith, H. Schouten, D. Yoerger, C. Palmiotto, A. Zhelezov, and H. Bai (2014), Sedimentation rates test models of oceanic detachment faulting, *Geophys. Res. Lett.*, in press.
- Petit, J. P. (1987), Criteria for the sense of movement on fault surfaces in brittle rocks, *J. Struct. Geol.*, **9**, 597–608.
- Reston, T. J., and C. R. Ranero (2011), The 3-D geometry of detachment faulting at mid-ocean ridges, *Geochem. Geophys. Geosyst.*, **12**, Q0AG05, doi:10.1029/2011GC003666.
- Schouten, H., D. K. Smith, J. R. Cann, and J. Escartin (2010), Tectonic versus magmatic extension in the presence of core complexes at slow-spreading ridges from a visualization of faulted seafloor topography, *Geology*, **38**, 615–618, doi:10.1130/G30803.1.
- Schroeder, T. J., M. Cheadle, H. J. B. Dick, U. Faul, J. F. Casey, and P. B. Kelemen (2007), Non-volcanic seafloor spreading and corner-flow rotation accommodated by extensional faulting at 15°N on the Mid Atlantic Ridge: A structural synthesis of ODP Leg 209, *Geochem. Geophys. Geosyst.*, **8**, Q06015, doi:10.1029/2006GC001567.
- Searle, R. C., M. Cannat, K. Fujioka, C. Mevel, H. Fujimoto, A. Bralee, and L. Parson (2003), FUJI Dome: A large detachment fault near 64°E on the very slow-spreading Southwest Indian Ridge, *Geochem. Geophys. Geosyst.*, **4**(8), 9105, doi:10.1029/2003GC000519.
- Searle, R. C., et al. (2010), Structure and development of an axial volcanic ridge: Mid-Atlantic Ridge, 45°N, *Earth Planet. Sci. Lett.*, **299**(1–2), 228–241.
- Smith, D. K., and J. R. Cann (1993), Building the crust at the Mid-Atlantic Ridge, *Nature*, **365**, 707–715.
- Smith, D. K., J. Escartin, M. Cannat, M. Tolstoy, C. G. Fox, D. Bohnenstiehl, and S. Bazin (2003), Spatial and temporal distribution of seismicity along the northern Mid-Atlantic Ridge (15°–35°N), *J. Geophys. Res.*, **108**(B3), 2167, doi:10.1029/2002JB001964.

- Smith, D. K., J. R. Cann, and J. Escartin (2006), Widespread active detachment faulting and core complex formation near 13°N on the Mid-Atlantic Ridge, *Nature*, *442*, 440–443, doi:10.1038/nature04950.
- Smith, D. K., J. Escartin, H. Schouten, and J. R. Cann (2008), Fault rotation and core complex formation: Significant processes in seafloor formation at slow-spreading mid-ocean ridges (Mid-Atlantic Ridge, 13–25°N), *Geochem. Geophys. Geosyst.*, *9*, Q03003, doi:10.1029/2007GC001699.
- Spencer, J. E. (1999), Geologic continuous casting below continental and deep-sea detachment faults and at the striated extrusion of Sacsayhuaman, Peru, *Geology*, *27*, 327–330.
- Thibaud, R., P. Gente, and M. Maia (1998), A systematic analysis of the Mid-Atlantic Ridge morphology and gravity between 15°N and 40°N: Constraints of the thermal structure, *J. Geophys. Res.*, *103*, 24,223–24,243.
- Tucholke, B. E., J. Lin, and M. C. Kleinrock (1998), Megamullions and mullion structure defining oceanic metamorphic core complexes on the mid-Atlantic ridge, *J. Geophys. Res.*, *103*, 9857–9866.
- Tucholke, B. E., M. D. Behn, W. R. Buck and J. Lin (2008), Role of melt supply in oceanic detachment faulting and formation of megamullions, *Geology*, *36*, 455–458, doi:10.1130/G24639A.1.
- Wessel, P., and W. H. F. Smith (1991), Free software helps map and display data, *Eos Trans. AGU*, *72*, 441–446.
- Wong, M. S., and P. B. Gans (2008), Geologic, structural, and thermochronologic constraints on the tectonic evolution of the Sierra Mazatán core complex, Sonora, Mexico: New insights into metamorphic core complex formation, *Tectonics*, *27*, TC4013, doi:10.1029/2007TC002173.